In Situ Monitoring of Electric Field Distribution in Mouse Tumor during Electroporation[1]

Matej Kranjc, PhD
Boštjan Markelc, PhD
Franci Bajd, PhD
Maja Čemažar, PhD
Igor Serša, PhD
Tanja Blagus, BSc
Damijan Miklavčič, PhD

Purpose: To investigate the feasibility of magnetic resonance (MR) electric impedance tomography (EIT) technique for in situ monitoring of electric field distribution during in vivo electroporation of mouse tumors to predict reversibly electroporated tumor areas.

Materials and Methods: All experiments received institutional animal care and use committee approval. Group 1 consisted of eight tumors that were used for determination of predicted area of reversibly electroporated tumor cells with MR EIT by using a 2.35-T MR imager. In addition, T1-weighted images of tumors were acquired to determine entrapment of contrast agent within the reversibly electroporated area. A correlation between predicted reversible electroporated tumor areas as determined with MR EIT and areas of entrapped MR contrast agent was evaluated to verify the accuracy of the prediction. Group 2 consisted of seven tumors that were used for validation of radiologic imaging with histopathologic staining. Histologic analysis results were then compared with predicted reversible electroporated tumor areas from group 1. Results were analyzed with Pearson correlation analysis and one-way analysis of variance.

Results: Mean coverage ± standard deviation of tumors with electric field that leads to reversible electroporation of tumor cells obtained with MR EIT ($38\% \pm 9$) and mean fraction of tumors with entrapped MR contrast agent ($41\% \pm 13$) were correlated (Pearson analysis, $r = 0.956$, $P = .005$) and were not statistically different (analysis of variance, $P = .11$) from mean fraction of tumors from group 2 with entrapped fluorescent dye ($39\% \pm 12$).

Conclusion: MR EIT can be used for determining electric field distribution in situ during electroporation of tissue. Implementation of MR EIT in electroporation-based applications, such as electrochemotherapy and irreversible electroporation tissue ablation, would enable corrective interventions before the end of the procedure and would additionally improve the treatment outcome.

© RSNA, 2014

Radiology

Monitoring of the electroporation process represents one of the most important aspects in the safe and efficient use of electroporation in clinical procedures (1), such as electrochemotherapy (2,3) and irreversible electroporation tissue ablation (4,5). Different approaches have already been suggested: electric conductivity measurement with electric impedance tomography (EIT) (6,7), voltage and current measurements of delivered pulses (8), magnetic resonance (MR) imaging (9,10), and ultrasonography (5,11). However, they are limited solely to irreversible electroporation applications (5,11), are unable to be used to monitor the process during pulse delivery (9,10), and can lead to inaccurate results (8), thus preventing control of the procedure and not allowing potential corrective intervention.

The safety and effectiveness of clinical applications of electroporation can be improved by introducing patient-specific pretreatment plans (12) (ie, an approach using numeric modeling to predict electroporation in a treated tissue). Nevertheless, the pretreatment plan cannot ensure tissue coverage with the required electric field, as it relies on the tissue electric conductivity and electrode placement data, to which electric field distribution is highly sensitive (13). Therefore, a new in situ monitoring approach is needed to increase efficiency and assume best possible clinical outcome of electroporation-based clinical procedures, which currently lack real-time monitoring.

Since accurate coverage of tissues with sufficiently large electric fields is important for successful electroporation (14,15), a method for determining electric field distribution based on MR EIT (16) was recently suggested. MR EIT enables reconstruction of electric field distribution by measuring the electric current density distribution and electric conductivity of the treated subject during application of electric pulses by using MR imaging and numeric algorithms. Feasibility of this method has been demonstrated in the determination of the electric field distribution in an agar phantom (16) and in liver tissue ex vivo (17). Therefore, the purpose of our study was to investigate the feasibility of MR EIT technique for in situ monitoring of electric field distribution during in vivo electroporation of mouse tumors to predict reversibly electroporated tumor areas.

Materials and Methods

Investigation of the feasibility of MR EIT for in situ monitoring of the electric field distribution during in vivo reversible electroporation of mouse tumors was performed in 15 tumors that were divided into two groups.

Group 1 consisted of eight tumors that were used for determination of the electric field distribution during electroporation. Five tumors (t_{1-5}) were subject to an electroporation protocol and contrast agent injections, while three tumors (t_{c1-c3}) were used for control; two of them received only injection of the contrast agent (t_{c1-c2}), while one was left completely intact (t_{c3}).

Group 2 consisted of seven tumors that were used for validation of radiologic imaging with histopathologic staining. Five tumors (t_{6-10}) were subject to the electroporation protocol and fluorescent dye injections, while two tumors (t_{c4-c5}) were used for control; one of them received only injection of the fluorescent dye (t_{c4}), while one was injected with vehicle only (t_{c5}).

Mice and Tumor Model

All animal experiments were conducted in accordance with the guidelines for animal experiments of the European Union directives, and permission was obtained from the Ministry of Agriculture and the Environment of the Republic of Slovenia (permission no. 34401–43/2011/5). A/J mice were purchased from the Medical Experimental Centre, Institute of Pathology, Faculty of Medicine, University of Ljubljana, Slovenia. Experiments were performed on male mice, 12–14 weeks old and weighing 22–26 g. Murine fibrosarcoma SA-1 (Jackson Laboratory; Bar Harbor, Maine) tumor cells were obtained from the ascitic form of the tumors in donor mice. For tumor induction, a suspension of tumor cells (1 ×

Advances in Knowledge

- Electric field distribution can be determined in situ during in vivo tissue electroporation by using MR electric impedance tomography (EIT).

- MR EIT can be used for prediction of reversibly electroporated areas in treated tissue; the method could also be applied for prediction of irreversibly electroporated areas.

Implication for Patient Care

- Implementation of MR EIT in electroporation-based applications such as electrochemotherapy and irreversible electroporation tissue ablation would enable corrective interventions before the end of procedure and additionally increase efficiency of the treatment—especially electrochemotherapy, which is currently deprived of real-time monitoring.

10^6 cells per milliliter) was prepared in 0.9% NaCl. Solid subcutaneous tumors were inoculated above the calf muscles of the hind leg with a subcutaneous injection of 50 µL of the prepared cell suspension. One tumor was inoculated per mouse.

Mice from group 1 were anesthetized with intraperitoneal injection of ketamine (1 mg/mL, Narketan; Vetoquinol, Ittigen, Switzerland), xylazine (5 mg/mL, Chanazine; Chanelle Pharmaceuticals Manufacturing, Loughrea, Ireland), and acepromazyne (0.4 mg/mL, Promace; Fort Dodge Animal Health, Kansas City, Mo), while group 2 mice were anesthetized with inhalation anesthesia with isofluorane flow rate 1%/L oxygen (Isofluorane; Nicholas Piramal India, London, England).

Electroporation Protocol

Electroporation was performed by applying two sequences of four high-voltage electric pulses with an amplitude of 500 V and duration of 100 µsec at a pulse repetition rate of 5 kHz by using customized Cliniporator Vitae (IGEA, Carpy, Italy). The pulses were delivered via two self-built cylindrically shaped platinum-iridium electrodes inserted into the tumor. Each electrode was 1 mm in diameter, and the distance between them was between 3 and 4 mm, depending on the size of the tumor.

MR EIT

MR EIT is an MR imaging modality based on the current density imaging pulse sequence for visualization of an electric conductivity distribution inside a conductive sample (18). Current density imaging is an MR imaging sequence that enables imaging of electric currents via magnetic field change induced by the currents (19,20). During the electroporation protocol, a 2.35-T MR imager (100-MHz proton nuclear MR frequency; Oxford Instruments, Abingdon, London) equipped with microimaging accessories with maximum gradients of 250 mT/m (Bruker, Ettlingen, Germany) acquired signal phase shifts that are proportional to the magnetic field change caused by

electric current flowing through the tumor. Magnetic field changes induced by electric pulses were acquired with the two-shot rapid acquisition with relaxation enhancement current density imaging sequence (21) with the following parameters: field of view, 30 mm; imaging matrix, 64 × 64; inter-echo delay, 2.64 msec; and echo time for the current encoding period, 20 msec. MR EIT J-substitution algorithm (22) was applied for reconstruction of electric conductivity and electric field distribution in the tumor. This mathematic process has been described in detail previously (16). From the obtained electric field distribution, a surface area with electric field distribution ranging from reversible (400 V/cm) to irreversible (900 V/cm) electroporation threshold value, (ie, predicted area of reversibly electroporated tumor cells) was determined. Finally, coverage C_{MREIT} was calculated by dividing the predicted surface area of the reversibly electroporated tumor cells by the surface area of the entire tumor.

MR Imaging Contrast Agent and Acquisition

The contrast agent gadolinium tetraazacyclododecane tetraacetic acid meglumine (Gd-DOTA, Dotarem; Guerbet, Aulnay-sous-Bois, France) was used for assessment of reversibly electroporated areas in the tumor by means of MR imaging. Gd-DOTA was injected intraperitoneally at the dose 10 mL per kilogram of a diluted solution isosmotic to plasma (1 mL of Gd-DOTA and 2.77 mL of water) 20 minutes before the application of electric pulses. T1-weighted images were acquired 24 hours after the electroporation protocol was performed and were expected to show the tumor areas where Gd-DOTA molecules were trapped inside the reversibly electroporated tumor cells. Quantification of trapped Gd-DOTA was achieved by determining the area with signal intensity higher than $S_{Gd-DOTA} = S_m + (2 \cdot SD_m)$, where S_m is the mean signal intensity in a region of a mouse leg that was not affected by electric pulses and SD_m

is the standard deviation (23). Tumor fraction $F_{Gd-DOTA}$ was then calculated by dividing the surface area of reversibly electroporated tumor cells by the surface area of the entire tumor.

MR imaging was performed with the same system as in MR EIT. T1-weighted MR images were obtained by using a T1-weighted spin-echo sequence with the following parameters: repetition time msec/echo time msec, 412/10; spectral width, 100 kHz; four accumulations; isotropic in-plane spatial resolution, 117 × 117 µm; and section thickness, 4 mm. The total acquisition time was 7 minutes.

Fluorescent Dye

Cell membrane–impermeable fluorescent dye Lucifer yellow (LY) (dilithium salt; Sigma-Aldrich, St Louis, Mo) was used for evaluation of LY distribution within electroporated tumor. LY was diluted in distilled water (vehicle) to a final concentration of 1 mmol/L, and 50 µL of LY solution was injected intratumorally immediately before the electroporation protocol. At the time point of 15 minutes posttreatment, mice were sacrificed, and tumors were collected.

Histologic Analysis

The collected tumors were fixed in paraformaldehyde for 24 hours and stored in 70% ethanol until they were embedded in paraffin. Two consecutive 1-µm-thick sections were cut in three parallel planes of the tumor in the direction perpendicular to the electrodes to obtain representative samples from different parts of the tumor (periphery and center). The first section was stained with hematoxylin-eosin, and the other one was first used for LY fluorescence observation and afterward for immunohistochemical staining. The sections for immunohistochemical staining were first incubated with rabbit polyclonal antibodies against LY (Antilucifer yellow; Life Technologies, Grand Island, NY) at a dilution of 1:2000. Second, a peroxidase conjugated streptavidin-biotin system (rabbit-specific HRP/DAB detection IHC kit, ab64261; Abcam,
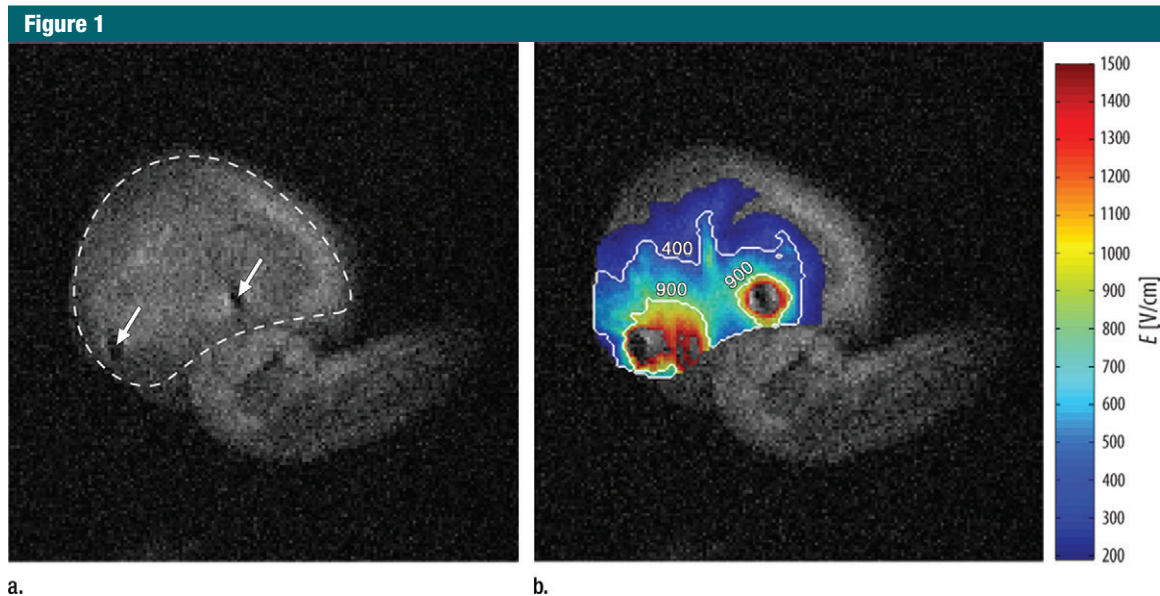
Figure 1

a.   b.

Figure 1: MR EIT images demonstrate electric field distribution in a mouse tumor during electroporation. **(a)** The tumor t_1 (marked with a dashed white line) is situated on an animal leg in this T1-weighted image, acquired in the section perpendicular to the electrodes. Locations of the two inserted electrodes are marked with arrows. **(b)** The electric field distribution in the tumor, obtained with MR EIT, was superimposed onto the T1-weighted image acquired before the application of electric pulses. A white contour line encloses an area exposed to an electric field strength between reversible (400 V/cm) and irreversible (900 V/cm) electroporation threshold values. Tumor cells located outside the area are either irreversibly electroporated (the area close to the electrodes) or remain unelectroporated (the area toward the tumor boundary).

Table 1

Coverage of Tumors with Reversibly Electroporated Tumor Cells Determined with MR EIT and Tumor Fractions with Entrapped Gd-DOTA

Tumor	C_{MREIT} (%)	$F_{Gd\text{-}DOTA}$ (%)
t_1	29.8	28.0
t_2	29.0	30.3
t_3	49.2	51.8
t_4	45.8	51.7
t_5	37.2	45.4
t_{c1}	0*	0*
t_{c2}	0*	0*
t_{c3}	0†	0†

Note.—Coverage C_{MREIT} and tumor fraction $F_{Gd\text{-}DOTA}$ were calculated by dividing the surface area of the reversibly electroporated tumor region and the surface area enclosing image pixels that exceeded $S_{Gd\text{-}DOTA}$ by the surface area of the entire tumor, respectively. The mean coverage (C_{MREIT}) of tumors (t_{1-5}) exposed to electric field that leads to reversible electroporation of tumor cells and the mean tumor fraction ($F_{Gd\text{-}DOTA}$) of tumors with entrapped Gd-DOTA were 38% ± 9 and 41% ± 13, respectively.

* Control tumors t_{c1-2} received only injection of contrast agent and were not subjected to electric pulses.

† Control tumor t_{c3} was left completely intact.

Cambridge, Mass) was used as the colorogenic reagent, followed by hematoxylin counterstaining. Slides were observed under visible light (excitation wavelength, 460–490 nm; emission wavelength, long pass 510 nm) or fluorescence conditions with a BX-51 microscope (Olympus, Hamburg, Germany) equipped with a digital camera (DP72; Olympus). Tumor fractions F_{LYint} were then calculated by dividing the surface area of the LY-positive fluorescence in each tumor section by the surface area of the entire tumor section and were then averaged for each tumor.

Statistical Analysis

All results were analyzed and described statistically by using commercial software Matlab 2013b (Mathworks, Natick, Mass) and its Statistics Toolbox. Five tumors were used in each statistical analysis. All data were tested for normal distribution with the Shapiro-Wilk test. Correlation (r) between predicted reversible electroporated tumor areas

as obtained with MR EIT and areas of the entrapped MR contrast agent was evaluated with linear Pearson correlation analysis. One-way analysis of variance was performed to compare LY entrapment within electroporated areas (F_{LYint}), MR contrast agent entrapment within electroporated areas ($F_{Gd\text{-}DOTA}$), and predicted reversible electroporated tumor areas obtained with MR EIT (C_{MREIT}). A P value less than .01 was considered to indicate a significant difference.

Results

Electric Field Distribution Determined with MR EIT

Electric field distributions were obtained in all five tumors (t_{1-5}) from group 1. No electric field was determined in control tumors (t_{c1-c3}), since they were not exposed to electric pulses. An example of electric field distribution obtained with MR EIT is shown in Figure 1b, where it is overlaid on the T1-weighted image
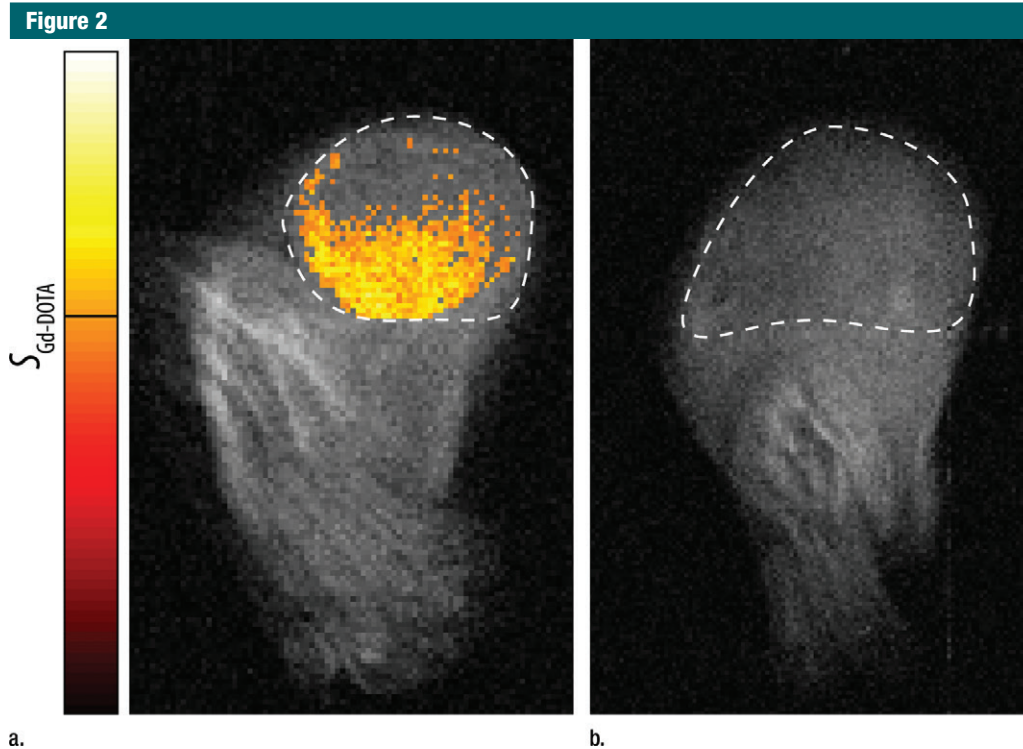
Figure 2

a.   b.

Figure 2: T1-weighted MR images of a leg section with a tumor in two mice 24 hours after injection of Gd-DOTA. On both images, the tumor is marked with a dotted white line. **(a)** Tumor t_1 was exposed to the electroporation protocol. Pixels on the T1-weighted MR image that exceeded $S_{Gd\text{-}DOTA}$—that is, tumor cells with entrapped Gd-DOTA—are visualized in color scale with the corresponding color bar on the left. **(b)** No electric pulses were applied to the tumor t_{c1}. Lack of Gd-DOTA in the tumor area was determined as reduced signal intensity that did not exceed $S_{Gd\text{-}DOTA}$. The same reduced signal intensity was also obtained for the rest of the control tumors (t_{c2}–t_{c3}). Pixel intensity values that were lower than $S_{Gd\text{-}DOTA}$ are not visualized in color scale for easier visualization of areas with entrapped Gd-DOTA.

acquired just before the application of electric pulses. The electric field was, as expected, highest around the electrodes, where it exceeded irreversible electroporation threshold (900 V/cm), while it remained under the reversible electroporation threshold (400 V/cm) in the areas away from electrodes. The mean coverage (C_{MREIT}) ± standard deviation of five tumors (t_{1-5}) with electric field that leads to reversible electroporation of tumor cells was 38% ± 9. As shown in Table 1, tumor coverage with reversibly electroporated tumor cells varied from one tumor to another but was in general between 30% and 50%.

Quantification of Entrapped Gd-DOTA within Reversibly Electroporated Areas

T1-weighted images of a leg section with a tumor in two mice that received Gd-

DOTA injection are shown in Figure 2. Results of Gd-DOTA electroporation–induced cell entrapment in tumors of mice that underwent Gd-DOTA injection and electric pulse application are presented together with coverage of tumors with electric field that leads to reversible electroporation of tumor cells in Table 1. The mean tumor fraction ($F_{Gd\text{-}DOTA}$) of five tumors with entrapped Gd-DOTA was 41% ± 13.

Correlation of Entrapped Gd-DOTA with Electric Field Determined with MR EIT

Correlation was evaluated between coverage of tumors with electric field that leads to reversible electroporation of tumor cells obtained with MR EIT (C_{MREIT}) and tumor fractions with entrapped Gd-DOTA ($F_{Gd\text{-}DOTA}$) with linear Pearson correlation analysis. Coverage of tumors with electric field

in the range of 400–900 V/cm, where reversible electroporation is expected, had good correlation with Gd-DOTA cell entrapment ($r = 0.956$, $P = .005$) as shown in Figure 3.

Quantification of Entrapped LY within Reversibly Electroporated Areas

For validation of radiologic imaging with histopathologic staining, staining of tumors with LY was used. Because of the preserved fluorescence of LY in paraffin tumor sections, evaluation of fluorescence intensity of LY in reversibly electroporated tumor cells was evaluated (Fig 4, *A*) and confirmed with immunohistologic staining of LY (Fig 4, *B* and *C*). In the tumor that was injected with vehicle only and not exposed to electric pulses (t_{c5}), no LY was observed; however, a high level of background staining was observed in
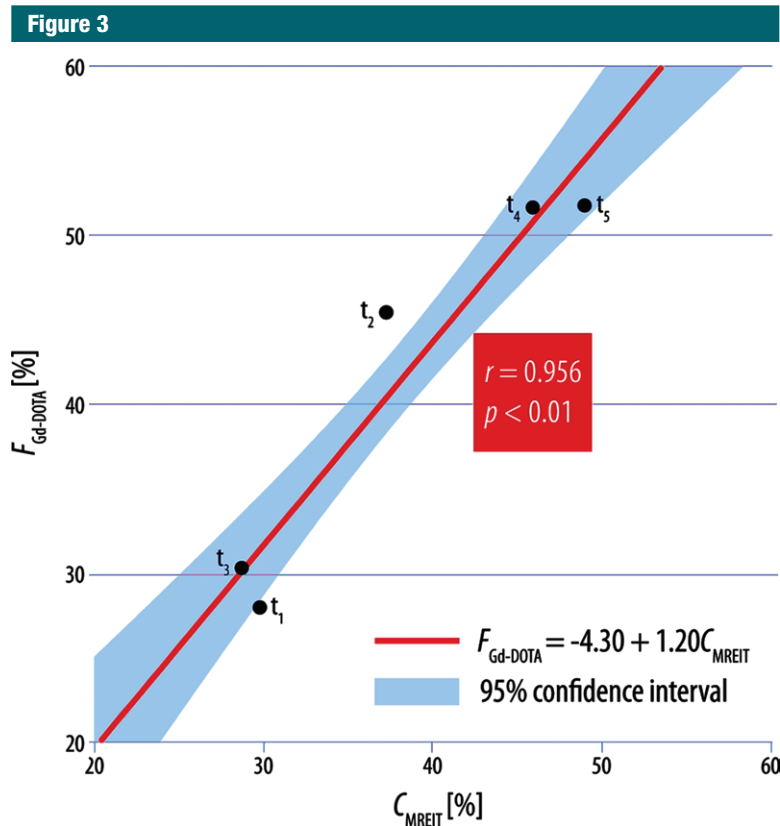
Figure 3: Scatterplot shows the coverage of tumors (t_{1-5}) with the electric field that leads to reversible electroporation of tumor cells (C_{MREIT}) and Gd-DOTA cell entrapment ($F_{Gd-DOTA}$). The regression line (red solid line) with the intercept $a = -4.30$ and slope $b = 1.20$ are shown together with 95% confidence interval (light blue area).

immunohistologically stained sections (Fig 4, *D–G*). The mean tumor LY-positive fraction (F_{LYint}) was higher in tumors that were exposed to electric pulses when compared with controls (Table 2). Mean tumor LY-positive fraction (F_{LYint}) was 39% ± 12. Mean tumor LY-positive fractions (F_{LYint}) in tumors from group 2 (t_{6-10}) were not statistically different from the coverage of tumors (t_{1-5}) with electric field that leads to reversible electroporation of tumor cells as determined with MR EIT (C_{MREIT}) and to tumor fractions with entrapped Gd-DOTA ($F_{Gd-DOTA}$) according to one-way analysis of variance ($P = .11$).

Discussion

In our study, we investigated the feasibility of the MR EIT technique for in situ monitoring of electric field distribution during in vivo electroporation of mouse tumors to predict reversible electroporation in tumor.

We successfully determined electric field distribution in situ during in vivo electroporation of the tumor. The determination was successful in all five tumors (t_{1-5}) from group 1, and areas of electric field that led to reversible electroporation of tumor cells obtained with MR EIT correlated well with the area of Gd-DOTA entrapment in cells. A concern of statistical significance may arise, owing to the small sample number of mouse tumors used for examination of this correlation. However, a sample size may be smaller for samples with correlation coefficients close to 1 to show a significant correlation (24).

Apparent differences can be observed when comparing tumor coverage with electric field that leads to reversible electroporation of tumor cells (C_{MREIT}). These can be attributed to a varying distance between the electrodes that lead to different electric field intensities in different tumors. Another source of varying electric field distribution can be heterogeneity of tumor electric conductivity (25). However, the advantage of MR EIT is exactly its ability to compensate for the effects of different electrode placements and tumor conductivity heterogeneities that occur in treated tissues, thus yielding accurate electric field distribution. Differences can be observed for most tumors in group 1 when comparing tumor fractions with entrapped Gd-DOTA ($F_{Gd-DOTA}$) and tumor coverages with electric field that leads to reversible electroporation of tumor cells (C_{MREIT}). This suggests that the predicted area of reversibly electroporated tumor cells was smaller than the area of Gd-DOTA entrapment in cells. Values for the reversible and irreversible threshold that were used in our study for determination of predicted area of reversibly electroporated tumor cells are commonly used in pretreatment planning for electrochemotherapy (12). These thresholds were estimated in previous studies by comparing in vivo measurements with numeric modeling of electroporation in subcutaneous tumors (26). Deviations from threshold values are expected and have been reported, especially for the irreversible threshold (27). When the area enclosing reversibly electroporated tumor cells is increased by setting the irreversible threshold to a higher value (940 V/cm), even better correlation was obtained between predicted electroporated tumor areas and areas of the entrapped MR contrast agent Gd-DOTA. Since electroporation thresholds for different tissues are still not well established, MR EIT might also play an important role in future studies in determining more accurate values of electroporation thresholds, which could increase the efficiency of pretreatment planning of procedures such as electrochemotherapy and irreversible electroporation ablation.

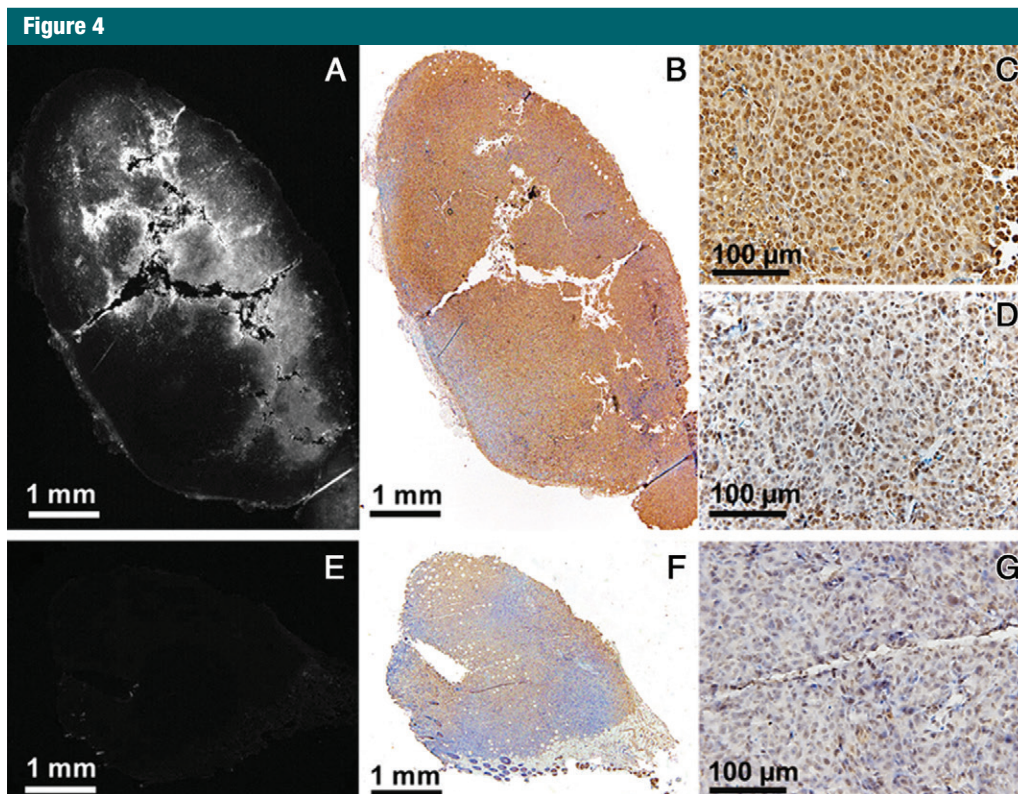To confirm the correlation between coverage of tumors with electric field

Figure 4: Representative *A*, fluorescence (original magnification, ×4) and, *B–G*, immunohistochemically stained (peroxidase conjugated streptavidin-biotin system with diaminobezidine as a chromogen and hematoxylin as a counterstain; original magnification for *B, E,* and *F*, ×4; original magnification for *C, D,* and *G*, ×40) images of tumors were acquired, *B–D*, 15 minutes after injection of LY and electroporation or, *E–G*, 15 minutes after injection of vehicle alone, where, *F, G*, the background staining is visible. Discrimination between, *C*, intense (positive) immunostaining of LY and, *D*, nonspecific staining was clearly evident.

Table 2

Percentage of Tumor Fraction with LY Entrapment

Tumor	F_{LYint} (%)
t_6	27.5 ± 8.4
t_7	58.9 ± 7.6
t_8	45.7 ± 2.0
t_9	30.8 ± 6.2
t_{10}	32.88 ± 5.6
t_{c4}	15.5 ± 5.4*
t_{c5}	0.4 ± 0.5†

Note.—Data are means ± standard deviations. Tumor fractions F_{LYint} were calculated by dividing the surface area of the LY-positive fluorescence in each tumor section by the surface area of the entire tumor section and then averaged for each tumor. The mean tumor LY-positive fraction (F_{LYint}) was 39% ± 12.

* Control tumor t_{c4} received only injection of the fluorescent dye.

† Control tumor t_{c5} was injected with the vehicle only.

that leads to reversible electroporation of tumor cells obtained with MR EIT (C_{MREIT}) and tumor fractions with entrapped Gd-DOTA ($F_{Gd-DOTA}$), histologic analysis was performed on additional tumors. We used an impermeable dye, LY, which does not enter the cells with intact cell membranes but enters the cells and becomes entrapped only in those cells that were exposed to reversible electroporation (28). For technical reasons, such as different time points of tumor evaluation, a direct comparison with radiologic imaging was not possible. Nevertheless, there were no significant differences between the mean tumor LY-positive fractions in tumor sections (F_{LYint}), tumor fractions with entrapped Gd-DOTA ($F_{Gd-DOTA}$), and coverage of tumors with the electric field that leads to reversible electroporation of tumor cells (C_{MREIT}), providing

convincing evidence for a correct MR EIT prediction.

The main limitation of our study was related to the limited sample space of the available MR imaging unit. Namely, precise positioning of the mouse leg with tumor and inserted electrodes inside the closed MR imaging unit was difficult to achieve. Therefore, only relative comparison was possible by evaluating tumor fractions with entrapped Gd-DOTA and coverage of tumors with the electric field that led to reversible electroporation. Nevertheless, MR EIT was already successfully applied for in vivo measurement of electric conductivity of a human leg (29). Additional difficulties do arise when MR EIT is coupled with electroporation, as MR imaging units have limited capabilities for their use in interventional procedures. However,

a report on MR EIT with an open MR imaging unit makes implementation of MR EIT with electroporation in clinical settings feasible in the near future (30). Another difficulty associated with our study was the validation of radiologic imaging with histopathologic staining. Namely, there is no widely used histologic stain for determination of reversibly permeabilized cells. We decided to use LY, which is a cell membrane–impermeable dye that retains its fluorescence in formalin-fixed tissues and can be detected with the use of anti-LY antibodies. Although LY should not enter the viable cell, we obtained a high level of background staining in non-electroporated tumors, which could be due to several reasons. First, the tissue could be damaged by insertion of the electrodes. Second, excision of tumor, cutting it in half for further histologic preparation, could cause distribution of the LY along the cutting edge. Nevertheless, strong positive reaction was obtained in cell nucleus in viable cells of electroporated tumors, showing the areas of reversible electroporation, which also correlated well with electric field distribution determined with MR EIT.

In conclusion, our study shows that MR EIT can be used for the assessment of electric field distribution in situ during tissue electroporation. As accurate coverage of treated tissue with a sufficiently large electric field represents one of the most important conditions for successful electroporation, electric field distribution determined by means of MR EIT could be used as a predictive factor for electrochemotherapy and irreversible electroporation tissue ablation outcome. This method would be helpful in particular for electrochemotherapy, a procedure that is currently lacking real-time monitoring. Our future studies will focus on implementation of MR EIT in electroporation-based clinical applications, such as electrochemotherapy and irreversible electroporation tissue ablation, where it may be applied for corrective interventions before the end of the procedure and, thus, additionally improve the treatment outcome.

References

1. Yarmush ML, Golberg A, Serša G, Kotnik T, Miklavčič D. Electroporation-based technologies for medicine: principles, applications, and challenges. Annu Rev Biomed Eng 2014;16:295–320.

2. Marty M, Sersa G, Garbay JR, et al. Electrochemotherapy—an easy, highly effective and safe treatment of cutaneous and subcutaneous metastases: results of ESOPE (European Standard Operating Procedures of Electrochemotherapy) study. Eur J Cancer Suppl 2006;4(11):3–13.

3. Miklavčič D, Mali B, Kos B, Heller R, Serša G. Electrochemotherapy: from the drawing board into medical practice. Biomed Eng Online 2014;13(1):29.

4. Neal RE 2nd, Rossmeisl JH Jr, Garcia PA, Lanz OI, Henao-Guerrero N, Davalos RV. Successful treatment of a large soft tissue sarcoma with irreversible electroporation. J Clin Oncol 2011;29(13):e372–e377.

5. Lee EW, Chen C, Prieto VE, Dry SM, Loh CT, Kee ST. Advanced hepatic ablation technique for cr eating complete cell death: irreversible electroporation. Radiology 2010;255(2):426–433.

6. Hjouj M, Rubinsky B. Magnetic resonance imaging characteristics of nonthermal irreversible electroporation in vegetable tissue. J Membr Biol 2010;236(1):137–146.

7. Granot Y, Ivorra A, Maor E, Rubinsky B. In vivo imaging of irreversible electroporation by means of electrical impedance tomography. Phys Med Biol 2009;54(16):4927–4943.

8. Cukjati D, Batiuskaite D, André F, Miklavcic D, Mir LM. Real time electroporation control for accurate and safe in vivo non-viral gene therapy. Bioelectrochemistry 2007;70(2):501–507.

9. Mahmood F, Hansen RH, Agerholm-Larsen B, Jensen KS, Iversen HK, Gehl J. Diffusion-weighted MRI for verification of electroporation-based treatments. J Membr Biol 2011;240(3):131–138.

10. Guo Y, Zhang Y, Nijm GM, et al. Irreversible electroporation in the liver: contrast-enhanced inversion-recovery MR imaging approaches to differentiate reversibly electroporated penumbra from irreversibly electroporated ablation zones. Radiology 2011;258(2):461–468.

11. Schmidt CR, Shires P, Mootoo M. Real-time ultrasound imaging of irreversible electroporation in a porcine liver model adequately characterizes the zone of cellular necrosis. HPB (Oxford) 2012;14(2):98–102.

12. Edhemovic I, Brecelj E, Gasljevic G, et al. Intraoperative electrochemotherapy of colorectal liver metastases. J Surg Oncol 2014 Apr 30. [Epub ahead of print]

13. Kos B, Zupanic A, Kotnik T, Snoj M, Sersa G, Miklavcic D. Robustness of treatment planning for electrochemotherapy of deep-seated tumors. J Membr Biol 2010;236(1):147–153.

14. Miklavcic D, Corovic S, Pucihar G, Pavselj N. Importance of tumour coverage by sufficiently high local electric field for effective electrochemotherapy. Eur J Cancer Suppl 2006;4(11):45–51.

15. Miklavcic D, Beravs K, Semrov D, Cemazar M, Demsar F, Sersa G. The importance of electric field distribution for effective in vivo electroporation of tissues. Biophys J 1998;74(5):2152–2158.

16. Kranjc M, Bajd F, Serša I, Miklavčič D. Magnetic resonance electrical impedance tomography for monitoring electric field distribution during tissue electroporation. IEEE Trans Med Imaging 2011;30(10):1771–1778.

17. Kranjc M, Bajd F, Sersa I, Woo EJ, Miklavcic D. Ex vivo and in silico feasibility study of monitoring electric field distribution in tissue during electroporation based treatments. PLoS One 2012;7(9):e45737.

18. Seo JK, Woo EJ. Electrical tissue property imaging at low frequency using MREIT. IEEE Trans Biomed Eng 2014;61(5):1390–1399.

19. Joy M, Scott G, Henkelman M. In vivo detection of applied electric currents by magnetic resonance imaging. Magn Reson Imaging 1989;7(1):89–94.

20. Sersa I, Jarh O, Demsar F. Magnetic resonance microscopy of electric currents. J Magn Reson A 1994;111(1):93–99.

21. Sersa I. Auxiliary phase encoding in multi spin-echo sequences: application to rapid current density imaging. J Magn Reson 2008;190(1):86–94.

22. Kwon O, Woo EJ, Yoon JR, Seo JK. Magnetic resonance electrical impedance tomography (MREIT): simulation study of J-substitution algorithm. IEEE Trans Biomed Eng 2002;49(2):160–167.

23. Leroy-Willig A, Bureau MF, Scherman D, Carlier PG. In vivo NMR imaging evaluation

of efficiency and toxicity of gene electrotransfer in rat muscle. Gene Ther 2005;12(19): 1434–1443.

24. Hulley SB. Designing clinical research. Philadelphia, Pa: Wolters Kluwer/Lippincott Williams & Wilkins, 2013.

25. Muftuler LT, Hamamura MJ, Birgul O, Nalcioglu O. In vivo MRI electrical impedance tomography (MREIT) of tumors. Technol Cancer Res Treat 2006;5(4): 381–387.

26. Pavselj N, Bregar Z, Cukjati D, Batiuskaite D, Mir LM, Miklavcic D. The course of tissue permeabilization studied on a mathematical model of a subcutaneous tumor in small animals. IEEE Trans Biomed Eng 2005; 52(8):1373–1381.

27. Qin Z, Jiang J, Long G, Lindgren B, Bischof JC. Irreversible electroporation: an in vivo study with dorsal skin fold chamber. Ann Biomed Eng 2013;41(3):619–629.

28. Mir LM, Banoun H, Paoletti C. Introduction of definite amounts of nonpermeant molecules into living cells after electropermeabilization: direct access to the cytosol. Exp Cell Res 1988;175(1):15–25.

29. Kim HJ, Kim YT, Minhas AS, et al. In vivo high-resolution conductivity imaging of the human leg using MREIT: the first human experiment. IEEE Trans Med Imaging 2009;28(11):1681–1687.

30. Wang H, Wang Y, Yang W, Wang Z, Hu L. Conductivity image reconstruction of oblique slice with C-shaped open permanent magnet MRI systems. IEEE Trans Appl Supercond 2010;2 0(3):814–817.